TECHNICAL PAPER

Rolling V-groove microstructures on glass using a modified PDMS mold

Ming-Huai Hsu[1] · Yao-Yang Tsai[1] · Jhao-Hong Gao[1] · Sen-Yeu Yang[1]

Abstract

Unlike polymers, glass is prone to fracturing under localized stress during roll embossing. Molds traditionally used for glass embossing are rigid and unsuitable for roll embossing. In this investigation, we utilized a modified soft polydimethylsiloxane (PDMS) mold, known for its ease of fabrication and superior replication capacity, for roller embossing on glass. This innovation significantly cuts mold expenses while preserving PDMS's hydrophobic and low surface energy attributes. Consequently, it prevents adhesion between the glass and the mold during high-temperature embossing, ensuring that the demolding process does not harm the glass surface. We successfully carried out roll embossing on optical glass with a mere 1.65 mm thickness, using a self-devised stainless steel carrier plate and a mobile induction heating apparatus. This heating methodology departs from the conventional practice of employing multiple heat sources in glass embossing and instead uses a singular heat source. Induction heating is applied directly to the mold and 420 stainless steel carrier. The optical glass surface reaches a remarkably uniform temperature, with a minimal temperature differential of only 2.5 °C, which is highly advantageous for mobile roller embossing, resulting in a high replication rate of V-groove microstructures on glass.

Keywords Hot embossing · PDMS soft mold · Induction heating · Roller embossing · Magnetic particles · Glass

1 Introduction

Polymers, renowned for their lightweight nature and relatively lower glass transition temperatures (Tg), find frequent utilization in the production of hot-embossed optical components (Rezem et al. 2014; Sun et al. 2019). Conversely, glass materials are essential in creating high-precision optical components, primarily owing to their outstanding optical properties, including superior light transmittance, refractive index, dispersion, high-temperature resistance, chemical corrosion resistance, and moisture resistance, etc., and allow the glass to work under different environmental conditions makes it the first choice for various micro-optical applications (Hartmann et al. 2010; Luo et al. 2023).

V-groove optical microstructures are crucial in numerous optoelectronic products such as LED lights, LCDs, prism arrays, fiber optics, sensor devices, and integrated photonics (Fang et al. 2013; Bona et al. 2003; Zheng et al. 2011). Their function lies in the uniform distribution of light sources. Due to the non-linear direction of light after entering the diffusion plate, it is necessary to use a brightness-enhancement film (BEF) composed of V-groove optical microstructures to correct the direction of light propagation. This is achieved through the refraction and reflection of light, aiming to concentrate light beams and enhance brightness, increasing the viewing angle and improving the backlight efficiency of displays (Park et al. 2013; Zhao et al. 2013).

Apart from employing mechanical ultra-precision techniques, such as laser micromachining, ultrasonic vibration processing, and chemical etching, for the fabrication of glass microstructures (Haghbin et al. 2018; Corbari et al. 2013; Yan et al. 2002; Tan et al. 2016), hot embossing stands out as a cost-effective, high-quality method extensively applied in the production of optical element microstructures (Li et al. 2020, 2023; Hu et al. 2020). Unlike polymer embossing molds, selecting mold materials for embossing glass

✉ Sen-Yeu Yang
syyang@ntu.edu.tw

1 Department of Mechanical Engineering, National Taiwan University, Taipei 106, Taiwan

requires considering high-temperature resistance, hardness, thermal expansion coefficient, and excellent chemical stability.

Traditionally, mold materials, such as tungsten carbide (WC), silicon carbide (SiC), glassy carbon (GC), and stainless steel, are commonly used. Different from traditional molds, special glass embossing molds have their potential applications and advantages, such as silicon molds that are transparent to infrared wavelengths to facilitate CO_2 laser penetration heating and increase the surface temperature of the glass (Han et al. 2020), nickel-phosphorus (Ni-P) coating mold can produce large-area micron-scale microstructures (Zhou et al. 2011), fused silica wafer is used to manufacture component molds with micron- and nanoscale features (Yi et al. 2006), etc., all of which require the use of complex and expensive mold manufacturing technologies.

Temperature control plays a pivotal role in the hot embossing process for glass materials. It's imperative to synchronize the mold and glass heating to avoid sudden temperature differentials that could lead to glass breakage. Consequently, precise temperature regulation of the glass and the mold during embossing is critical, with a range of heating techniques at one's disposal. Traditional heating methods encompass a variety of heat sources, such as laser-assisted heat embossing with heater blocks (Lee et al. 2021), collaborative heating systems, infrared lamps, hot plates, and induction coils (Chen et al. 2015), as well as multifaceted heating systems, including ultrasonic vibration devices, heating furnaces, and infrared heaters (Tsai et al. 2012). The abovementioned aspects of glass embossing, including heating methods and mold selection, are all centered around the hot embossing process. Within this realm, heating techniques offer a wide range of choices. Multi-heat source heating is employed to mitigate temperature differentials between the glass and the mold during large-area embossing.

The development of roller-embossed optical glass stems from the susceptibility of flatbed hot embossing technology to uneven pressure distribution, resulting in inconsistent replication of microstructures and affecting the final product's dimensional accuracy (Sah et al. 2016). Moreover, the temperature fluctuation during the replication process can cause thermal expansion and contraction of the embossing substrate (Nievas et al. 2022). On the other hand, the roller-assisted embossing system employs a continuous embossing mechanism where materials pass through the embossing area continuously throughout the process. This technology can operate at high speeds because materials do not need to dwell in the embossing area for too long. The roller-assisted embossing system supports the continuity and efficiency of the entire process, making it particularly suitable for large-area production requirements (Atthi et al. 2021; Peng et al. 2023).

In our preceding investigations (Hsu et al. 2022, 2023a; Hsu et al.2023b), we observed significant alterations in the properties of PDMS, such as stiffness, hardness, thermal conductivity, and thermomechanical behavior, when incorporating magnetic particles into PDMS. Additionally, we explored the direct inductive heating of PDMS to create an internal heat source. In our current research, we combined a PDMS mold containing magnetic particles with a 420 stainless steel carrier, employing direct inductive heating for roller embossing. This approach uses a single induction heating device to enhance the temperature consistency between the mold and the glass, ensuring temperature uniformity, mitigating thermal stress, and boosting replication rates. The incorporation of magnetic particles into PDMS molds, while preserving PDMS's hydrophobic and low surface energy features, prevents glass from adhering to the molds at elevated temperatures. Consequently, demolding can be effortlessly executed without needing a release agent, eliminating the risk of harming the glass surface. Moreover, PDMS molds are straightforward to fabricate and offer superior mold replication capacity, considerably reducing the cost of glass embossing molds.

2 Experiments

2.1 Mold design and optical glass

The mold employed in this investigation consisted of a composite material made from 3.5 μm ultrafine nickel powder (T123, Vale S.A., BR) magnetic particles with a purity exceeding 99.8% and a 5:1 mixture of PDMS (SYLGARD 184, Dow Corning, USA). This combination resulted in a 70 wt% Ni-PDMS composite. After undergoing a curing and baking process at 85 °C for 24 h, the hardness of the mold reached an impressive Shore A 83HA, capable of withstanding roller embossing pressures of up to 7 kgf/cm² without deformation. The finished Ni-PDMS mold had a thickness of 4.0 mm and measured 60 mm × 60 mm in size, aligning with the dimensions of the optical glass employed for the embossing process. The optical glass utilized in this experiment is K-PG325 (Sumita Optical Glass, Inc., Japan), characterized by a Tg of 288 °C, with its thermal properties detailed in Table 1.

2.2 Thermal properties of magnetic particles embedded PDMS

Traditional PDMS molds are known for their softness, susceptibility to deformation under pressure, high thermal

Table 1 Thermal properties of K-PG325 optical glass

Property	Symbol	Value
Transition Temperature	Tg	288°C
Yield Point	At	317°C
Thermal Expansion	α	143×10^{-7} /°C (-30～+70°C)
		165×10^{-7} /°C (+50～+200°C)
Thermal Conductivity	λ	0.748 W. m^{-1}. k^{-1}
Specific Heat	Cp	817 J. kg^{-1}. k^{-1}

Table 2 Thermal conductivity measurement

Material	Thermal Conductivity (W/m.K)
Pure PDMS	0.15
Ni-PDMS (70 wt%)	0.54

Table 3 The coefficient of thermal expansion measurement

Material	CTE (α)
Pure PDMS	320E-6 /°C
Ni-PDMS (70 wt%)	228E-6 /°C

resistance, and poor thermal conductivity. When PDMS is heated for hot embossing, it typically relies on an external heat source. However, indirect heating from external heat sources often results in uneven temperature distribution on the PDMS surface, making it unsuitable for roller embossing.

This study aims to modify the thermal properties of PDMS itself directly, enhancing its thermal conductivity,

reducing internal thermal resistance, and ensuring uniform heat distribution. Additionally, we have changed the heating method to utilize internal heat sources and improve heating efficiency. The thermal conductivity of the mold plays a crucial role in determining the rate of temperature transfer within PDMS, which, in turn, influences the uniformity of temperature distribution. We measured the thermal conductivity of Ni-PDMS and pure PDMS using the hot flow plate method, as presented in Table 2. The results indicate a significant increase in the thermal conductivity of Ni-PDMS, which is 3.6 times that of pure PDMS (0.54 W/m·K compared to 0.15 W/m·K).

The coefficient of thermal expansion (CTE) is a primary consideration when selecting materials for glass embossing molds. If the CTE of the mold material is too high, it can lead to expansion and deformation of the microstructure during high-temperature imprinting, resulting in reduced dimensional accuracy. Therefore, we utilized a thermo-mechanical analyzer (TMA) to measure the CTE of Ni-PDMS. As shown in Table 3, adding nickel metal powder into PDMS reduced the thermal expansion coefficient from 320E-6 to 228E-6, marking an effective reduction of 29%. To further validate that the Ni-PDMS mold does not compromise the microstructure's dimensional accuracy due to thermal expansion, this study compared the microstructure's size with the dimensional replication rate and accuracy of
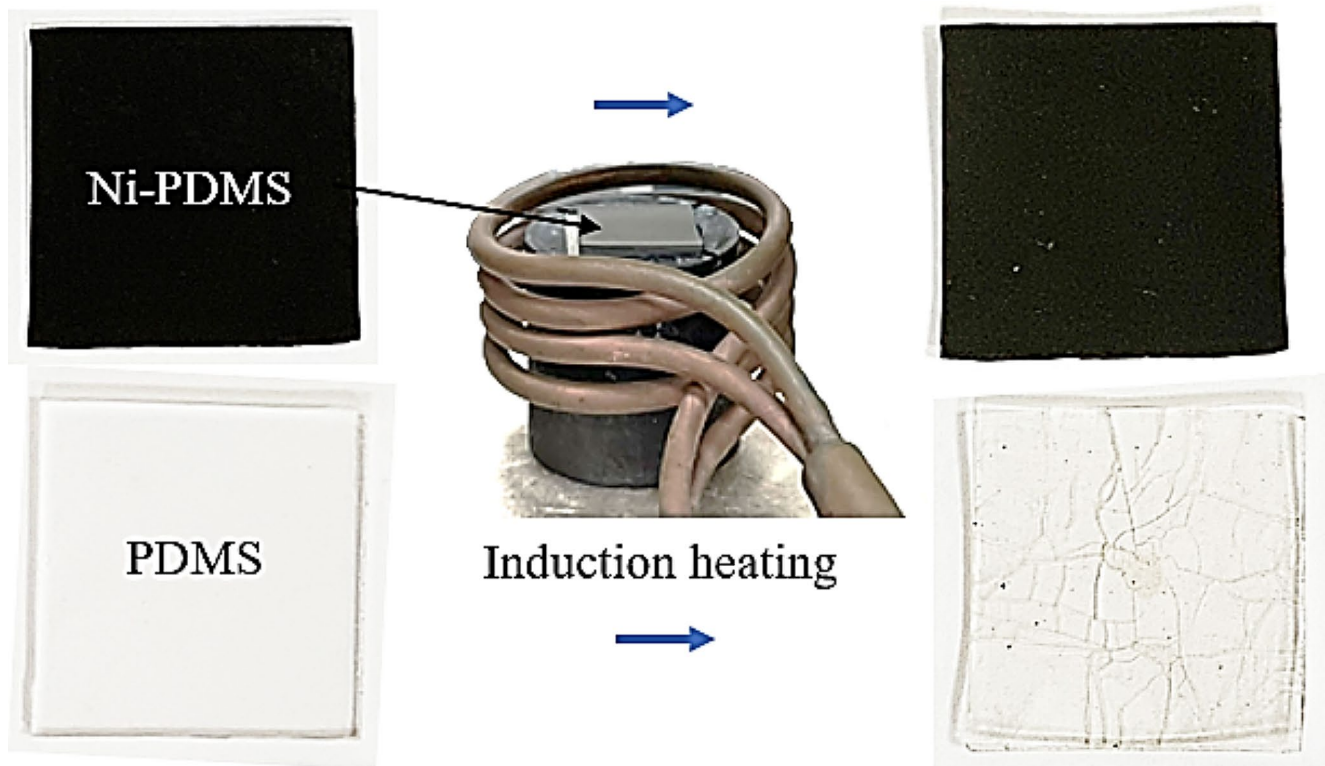
Fig. 1 PDMS produced severe cracks and shrinkage deformation after two heating and cooling cycles to 400 °C, while Ni-PDMS did not create any changes
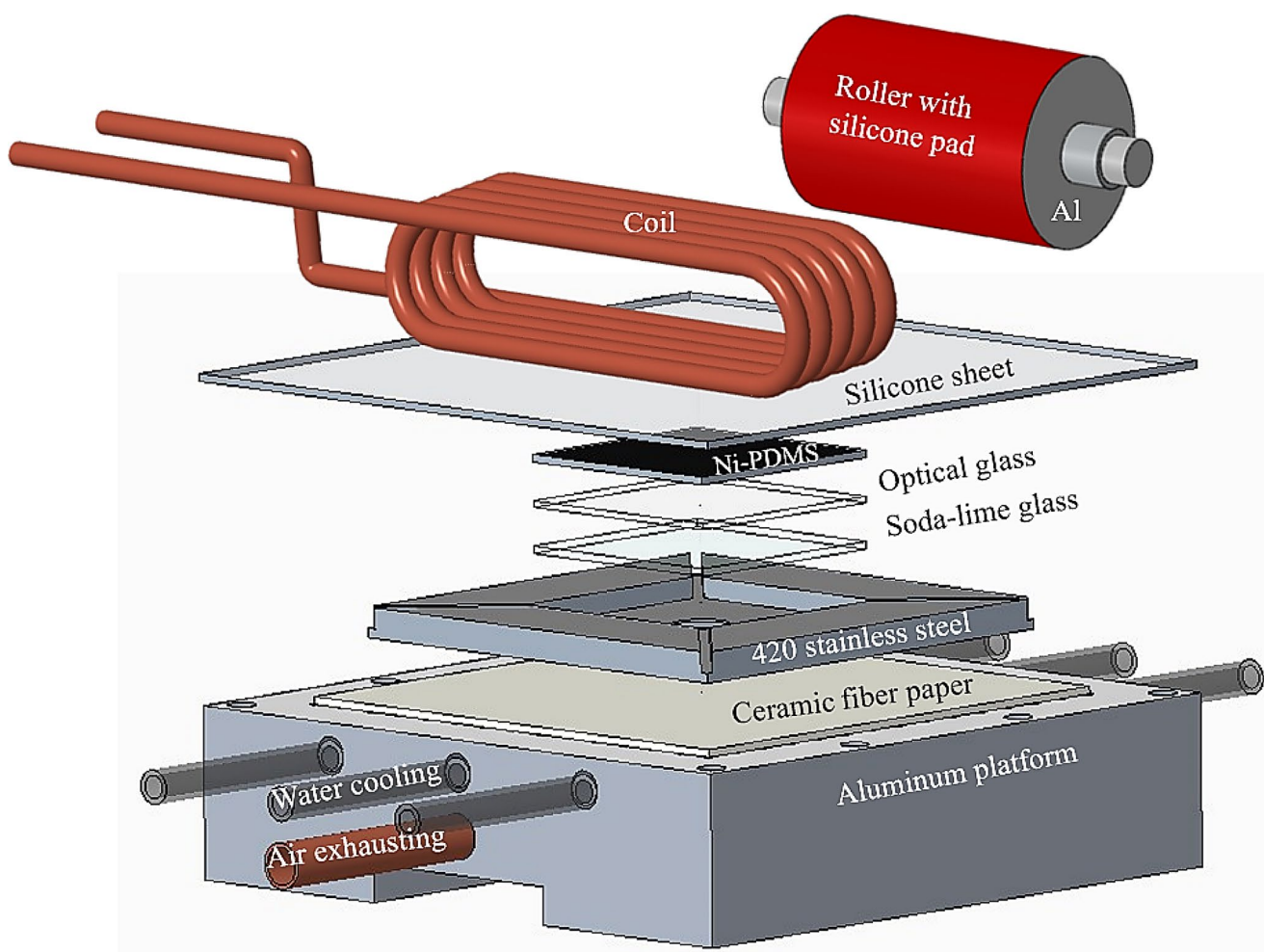
Fig. 2 Roller embossing platform design and embossing configuration diagram

embossed glass and verified these results through actual embossing.

PDMS molds are generally prepared with a mixing ratio of 10:1 of the AB agent, and their operational temperature range spans from − 55 to 200 °C. Consequently, pure PDMS is deemed unsuitable for high-temperature hot embossing processes exceeding 300 °C. However, to address this limitation, (Kim et al. 2013) adjusted the PDMS AB agent mixing ratio from 10:1 to 5:1, thus enhancing the thermal stability of the PDMS mold at temperatures reaching up to 300 °C, enabling hot embossing at elevated temperature levels. Additionally, Darwish and his team (Darwish et al. 2015) explored using a combination of primary agent A and curing agent B, with a 10:1 weight ratio and 20 wt% and 30 wt% magnetite to create Fe-PDMS composites. By employing a thermogravimetric analyzer (TGA), the researchers scrutinized the temperature stability of these two magnetite-PDMS composites with different mixing ratios. Their findings highlighted that incorporating magnetic powder into

pure PDMS can enable PDMS to withstand the demands at higher temperatures above 450℃.

Our study subjected 70 wt% Ni-PDMS composites and pure PDMS to induction heating experiments on iron blocks, assessing their performance at 400 °C. The results were striking, with pure PDMS exhibiting severe cracks and deformation after two heating and cooling cycles, as illustrated in Fig. 1. In stark contrast, Ni-PDMS remained entirely unaffected by these extreme conditions.

2.3 Platform design

The design and configuration of the platform for the optical glass embossing experiment are illustrated in Fig. 2. The aluminum platform is equipped with air extraction and water-cooling systems. This study employed natural cooling instead of water cooling to mitigate the rapid cooling risk of glass breakage. The air extraction system is designed to absorb breathable ceramic fiber paper and a silicone pad, securing the 420 stainless steel carrier, glass, and mold. This
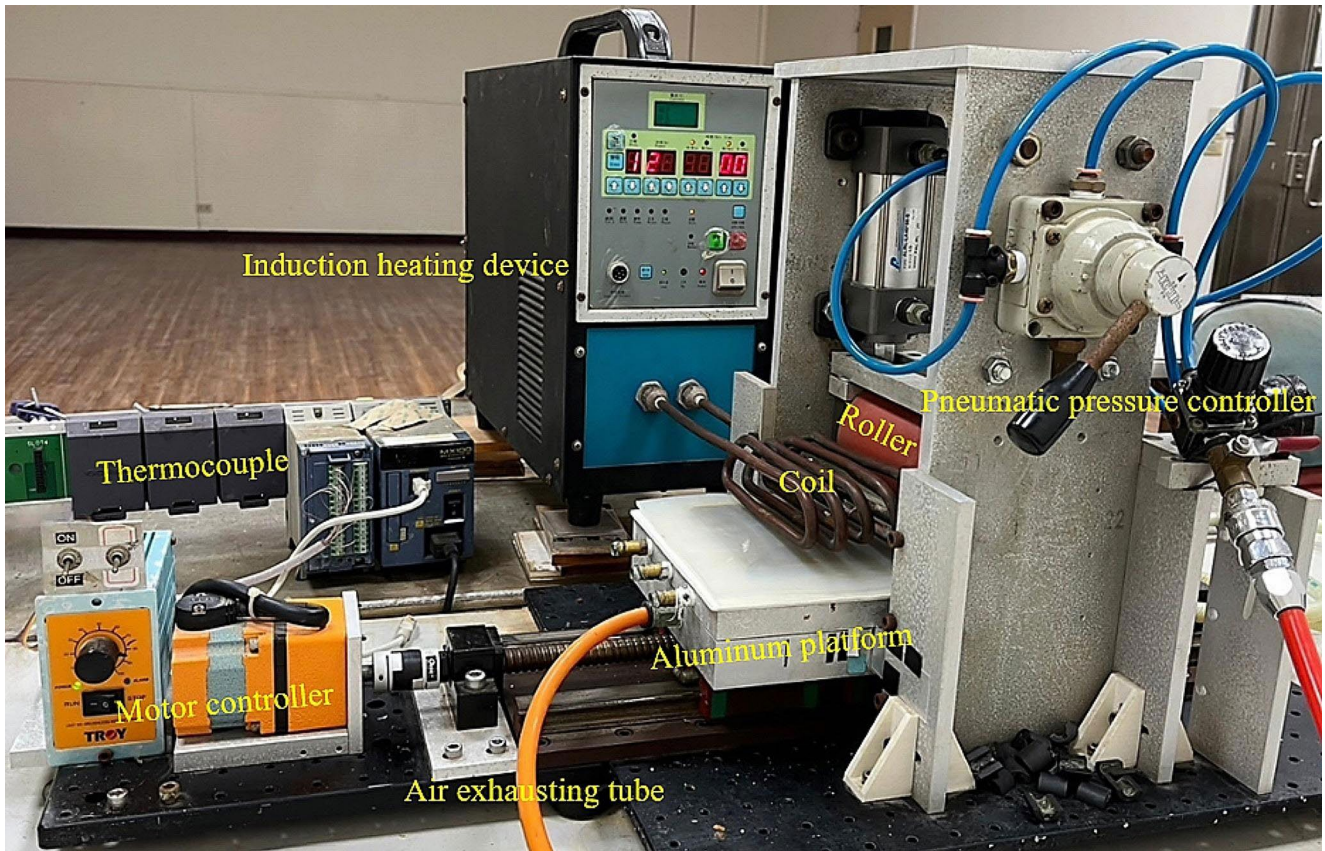
Fig. 3 Moving stage with induction heating roller system

system can ensure that the mold and glass remain stationary relative to each other during the roller embossing process. Ceramic fiber paper, withstanding temperatures up to 1260 °C, is a thermal insulation pad between the 420 stainless steel carrier and the aluminum stage.

The 120 mm × 120 mm × 8 mm stainless steel carrier features a 60 mm × 60 mm square groove, roughly matching the size of the optical glass to be embossed. The square
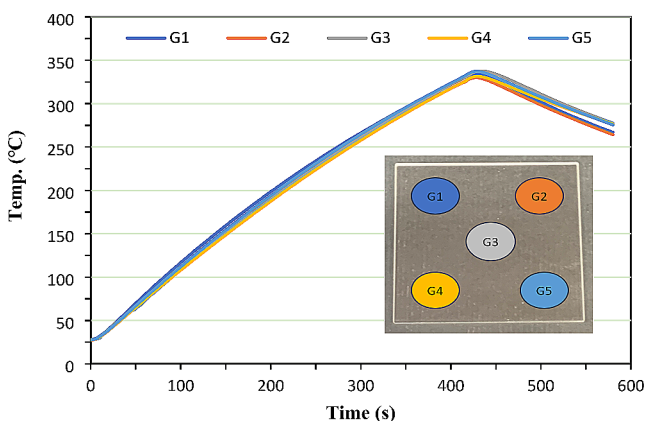
Fig. 4 Divide the surface of the optical glass into five areas and use thermocouple wires to measure the temperature records at these 5 points

groove, with a depth of 5.5 mm, induces cladding heating of the mold and glass during the induction heating process. The 420 stainless steel carrier includes four exhaust channels to prevent hot air from causing thermal expansion of the silicone pad at high temperatures. Optical glass with a Tg of 288 °C and a thickness of 1.65 mm is positioned between a Ni-PDMS mold and a soda-lime glass with a thickness of 2 mm and a Tg of 564 °C. Soda-lime glass, resistant to high temperatures, acts as a thermal conductor between stainless steel and optical glass. It ensures even heating and maintains the flatness of the optical glass substrate during the roller embossing process.
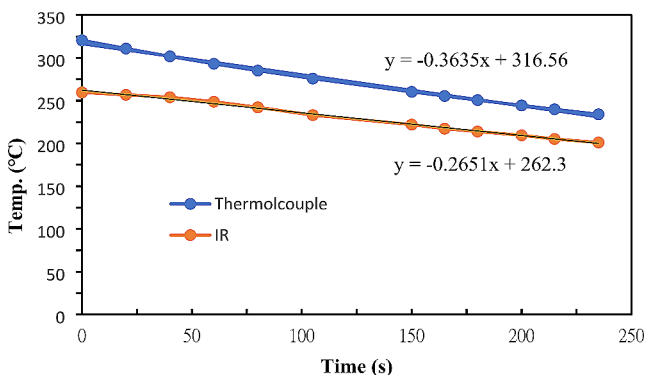
To prevent optical glass from cracking due to rigid roller embossing, the lower layer of soda-lime glass can increase the virtual thickness of the optical glass. Subsequently, the upper layer of optical glass is covered with a Ni-PDMS mold that is 4 mm thick, along with a high-temperature-resistant silicone pad that is 2 mm thick. Furthermore, the surface of the aluminum roller is wrapped with a 2 mm thick red silicone pad to serve as a buffer material during roller embossing.

(a)

(b)
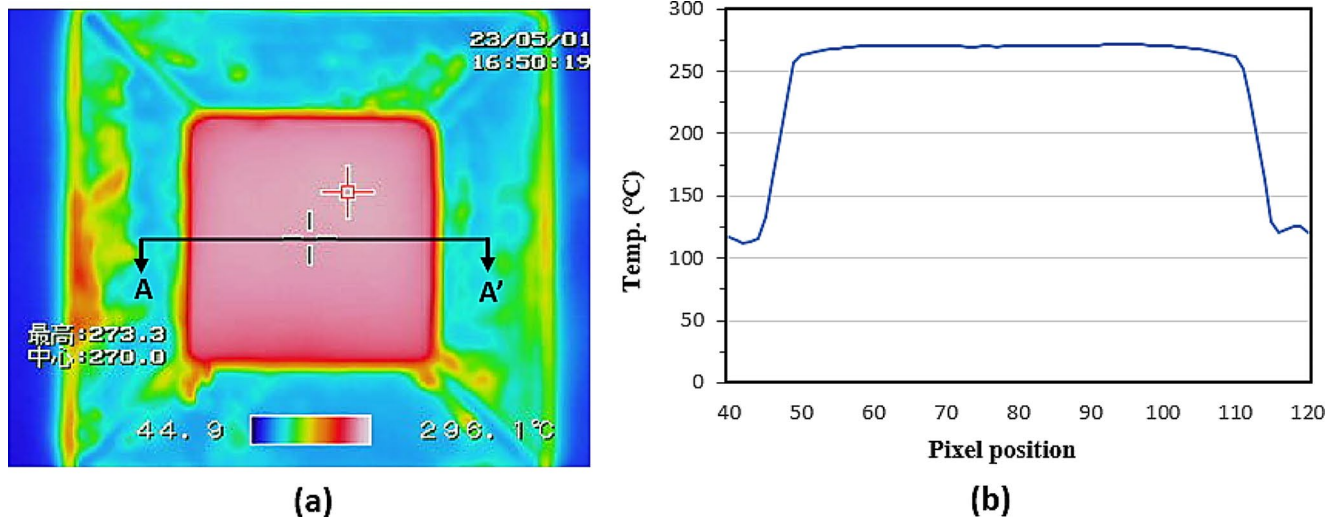
Fig. 5 **(a)** The infrared thermal imager captures a consistent temperature distribution across the surface of the Ni-PDMS mold. **(b)** The direct surface temperature measurements at the AA' section line reveal a minimal temperature disparity of only 2.5 °C between the highest and lowest points on the mold's surface. In contrast, the 420 stainless steel carrier exhibits a rapid cooling rate, a 150 °C temperature difference between itself and the Ni-PDMS mold

2.4 Moving and heating system design

The design and configuration of the mobile induction heating system are depicted in Fig. 3. The system uses a single heat source rather than multiple heat sources for heating. It can simultaneously inductively heat the 420 stainless steel carrier and Ni-PDMS mold. The experiment can be equipped with magnetic flux concentrators, enabling adjustment of the heating rate and temperature uniformity. The induction frequency is set at 80 kHz to gradually heat at 4.5 kW until it reaches an optimal embossing temperature of approximately 30 °C above the Tg of optical glass. Subsequently, the aluminum platform is moved beneath the roller to complete the embossing. The low-power, slow heating aims to achieve even temperature distribution on the glass surface. This approach can mitigate the risk of uneven
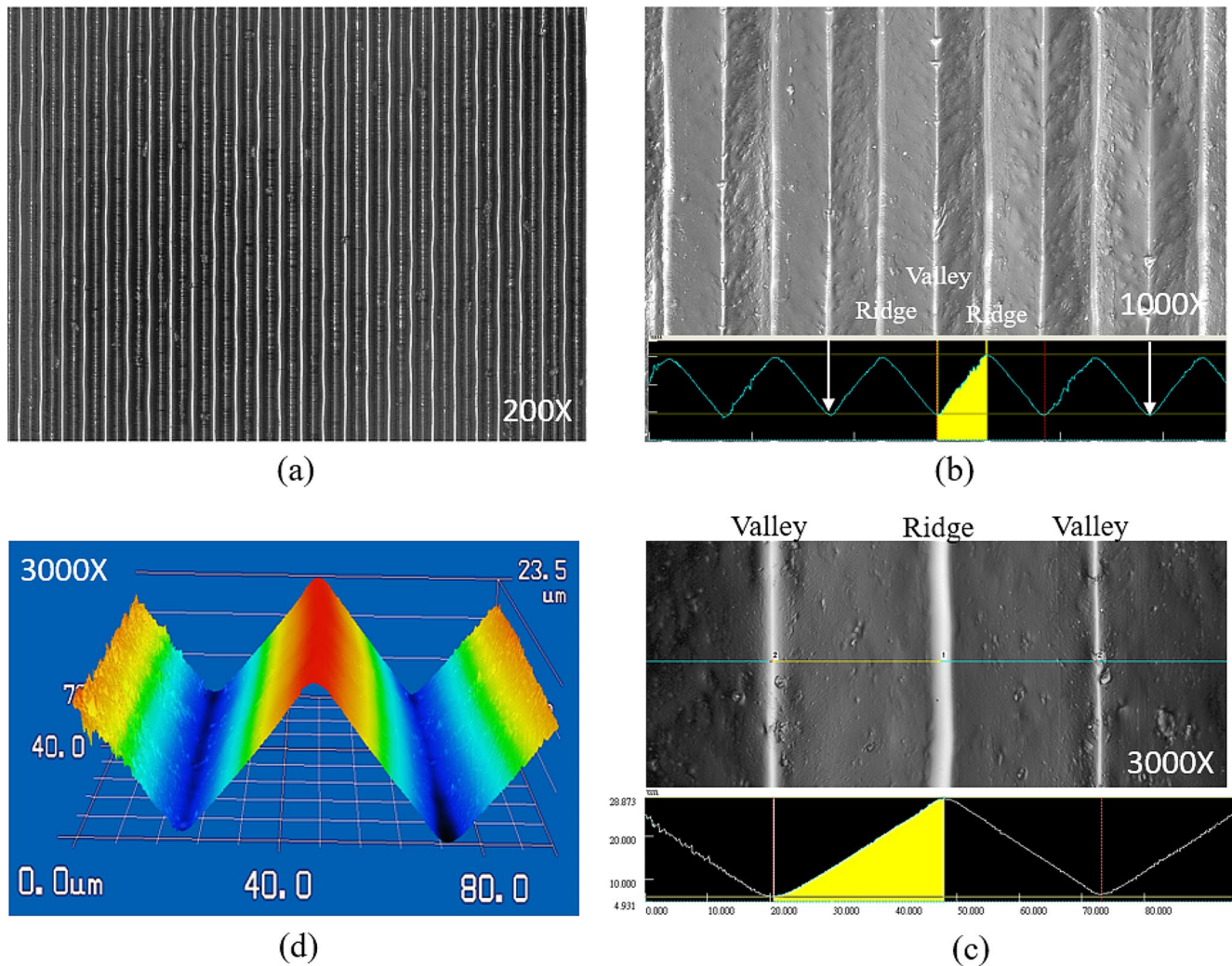
thermal stress distribution that rapid heating may induce, ultimately averting the potential for glass breakage.

3 Results and discussion

3.1 Thermocouple temperature measurement

Ensuring a consistent temperature distribution is pivotal in the intricate process of embossing. To validate that the average temperature of the optical glass surface falls within the optimal range of embossing temperature 320 to 335 °C, we employ temperature measurement techniques involving thermocouples and an infrared thermal imager. Despite the capability of the induction heating 420 stainless steel carrier for swift temperature elevation, our strategic preference leans towards a more controlled approach—utilizing a low-power 4.5 kW slow induction heating method characterized by an induction frequency of 80 kHz and a heating duration of 420 s. This deliberate choice safeguards against potential glass breakage from irregular heat distribution and thermal stress variations due to an excessively rapid temperature surge.

Upon cessation of the induction heating, the temperature exhibits a continued ascent, culminating around the 430s, accompanied by a heating rate of 0.72 °C/s, as portrayed in Fig. 4. The thermocouple wires facilitate precise contact temperature measurements, allowing us to directly evaluate the temperature at five specific points on the optical glass surface to confirm the uniformity of temperature across the optical glass surface and whether the optimal embossing temperature has been attained. Post the heating phase,

Fig. 6 The cooling rate for the optical glass surface using a thermocouple revealed a value of 0.36 °C/s, and the Ni-PDMS mold surface with an infrared thermal imager indicated a cooling rate of 0.27 °C/s

Fig. 7 The V-groove height of the embossed optical glass is measured using a LSCM. The magnifications are **(a)** 200X, **(b)** 1000X, **(c)** 3000X, and **(d)** 3000X 3D profile view

the platform progresses at a feed rate of 164 mm/min. The subsequent embossing procedure, executed using a roller, involves an embossing time of 22s for the whole Ni-PDMS mold. This approach ensures both the precision of temperature management and the efficacy of the embossing process.

3.2 Infrared thermal imaging camera

Thermocouple wires can directly measure the actual temperature on the glass surface. However, a non-contact infrared thermal imager is more suitable for a comprehensive temperature consistency and uniformity assessment. Figure 5(a) illustrates the surface temperature distribution of the Ni-PDMS mold and 420 stainless steel carrier captured by the infrared thermal imager. Notably, the temperature difference on the Ni-PDMS mold surface, excluding the contact part between the mold and stainless steel, is a mere 2.5 °C, showcasing a remarkably uniform distribution, as

depicted in Fig. 5(b). In contrast, the 420 stainless steel carrier exhibits a rapid cooling rate, resulting in a substantial temperature difference of nearly 150 °C between itself and the Ni-PDMS mold. This perspective underscores the role of the induction heating stainless steel carrier as the primary heat source. Nevertheless, the Ni-PDMS mold effectively elevates the glass surface temperature above Tg and maintains it until the rolling process is completed.

While the Ni-PDMS mold effectively sustains the glass surface temperature and regulates the cooling rate to uphold the optimal embossing temperature, it's important to note that the infrared thermal imager can only gauge the surface temperature of the Ni-PDMS mold. This measurement does not precisely mirror the actual temperature of the glass surface, and its accuracy is slightly inferior to a thermocouple.

While thermocouple wires offer a direct means to measure the actual temperature of the glass surface, their measurement method is relatively intricate compared to an
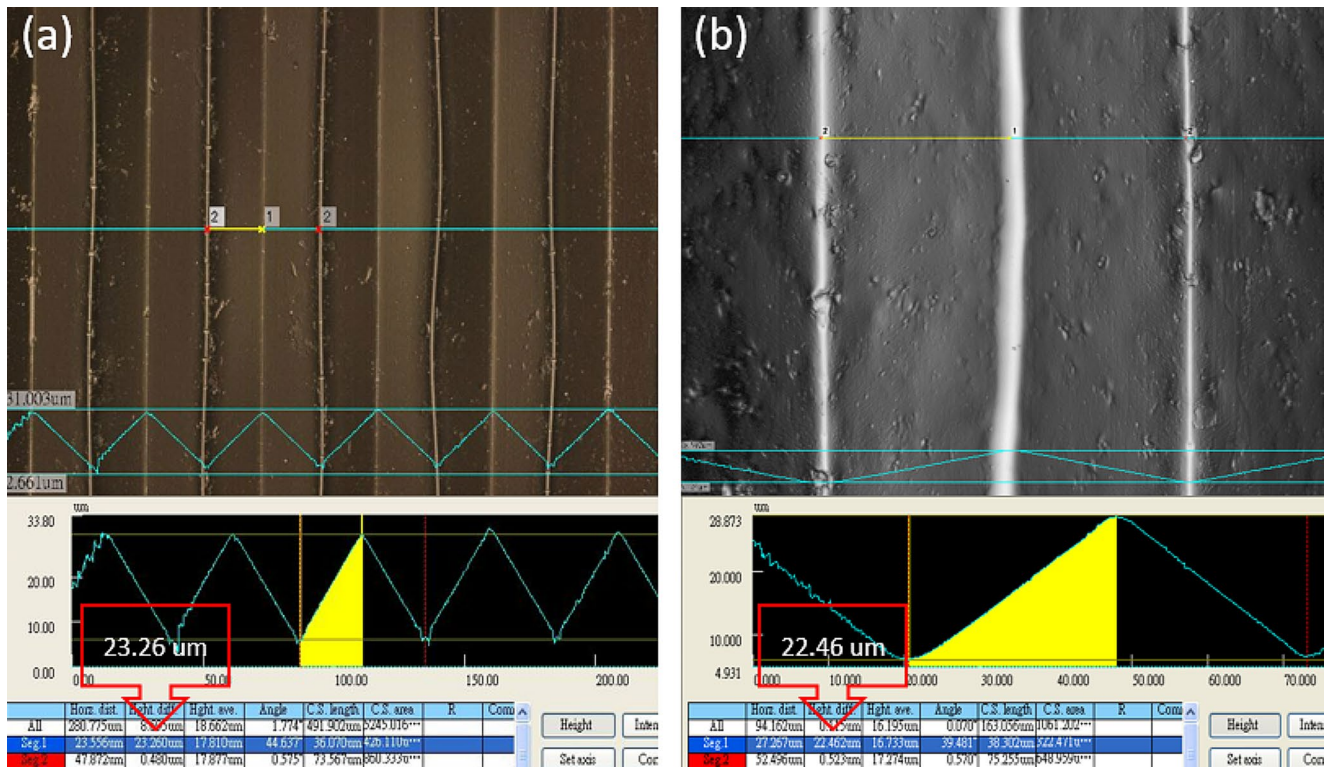
Fig. 8 **(a)** The V-groove thickness of the PDMS mold measured by LSCM is 23.26 μm, **(b)** and the thickness of the optical glass is 22.46 μm

infrared thermal imager. The contrast in surface temperatures between the optical glass and the Ni-PDMS mold, as observed through these two measurement methods, is approximately 42 °C, as illustrated in Fig. 6. The Ni-PDMS mold retains the high thermal resistance of PDMS, enabling the optical glass surface to cool at a slow rate of 0.36 °C/s, as depicted in Fig. 6. This is in contrast to stainless steel carriers, which cool rapidly. The difference in surface temperature between 420 stainless steel and Ni-PDMS molds is as high as 150 °C. The Ni-PDMS mold acts as a heat insulator to slow down the cooling rate of the optical glass. The cooling rate of its surface temperature measured through an infrared thermal imager is only 0.27 °C/s. It turns out that the slower cooling rate of Ni-PDMS is very beneficial for the moving roller embossing process.

3.3 Roller embossing

After the curing and baking process, the Ni-PDMS composite material achieves a hardness surpassing Shore A 83HA

and can withstand a rolling pressure of 7 kgf/cm² without deformation. Given the focus of this experiment on optical glass embossing and the necessity for enhanced protection for the optical glass, we opted to increase the thickness of the Ni-PDMS mold from 1.5 to 4 mm. Additionally, we used a 2 mm thick high-temperature silicone sheet to cover the Ni-PDMS mold. A red silicone pad, 2 mm in thickness, is utilized to cover the aluminum roller, acting as a buffer material to provide multi-layer protection for optical glass embossing. The roller pressure is critical when embossing optical glass with a thickness of 1.65 mm. Experimental findings indicate that a pressure of 3 kgf/cm² is the maximum limit for optical glass without risking breakage. A soda-lime glass with a Tg of 564 °C and a thickness of 2 mm is positioned beneath the optical glass. Apart from ensuring the non-embossed surface's flatness, it protects the optical glass and augments its effective virtual thickness.

We employed slow induction heating with a frequency of 80 kHz and a power of 4.5 kW. After heating for 420 s, we initiated the movement of the platform to start roller

Table 4 In the same temperature range, the average replication rate of 5 points on the optical glass corresponding to different embossing pressures

Pressure	Replication rate %					
kgf/cm²	G1	G2	G3	G4	G5	**AVG**
0.5	61.2%	58.7%	64.0%	72.5%	71.8%	**65.6%**
1	80.5%	77.3%	76.1%	84.2%	77.5%	**79.1%**
1.5	93.1%	95.2%	97.4%	95.7%	96.6%	**95.6%**
2	96.7%	92.7%	91.2%	92.9%	97.1%	**94.1%**

embossing with a feed rate of 164 mm/min. Rolling a 60 mm × 60 mm Ni-PDMS mold took approximately 22 s. Considering the glass surface cooling rate of 0.36 °C/s, the temperature during embossing could still be maintained within the optimal range of 320 to 335 °C. The embossing pressure is set between 0.5 and 2 kgf/cm². After rolling, natural cooling, and demolding, the embossed optical glass was divided into 5-point areas. A laser scanning confocal microscope (LSCM) was used to calculate the average replication rate. The magnification was 200 times, 1000 times, and 3000 times, respectively, to examine the height of the V-shaped groove and its profile, as shown in Fig. 7.

Finally, the measurement results are plugged into the calculation formula for the replication rate: replication rate % = (height of the V-groove on the patterned glass/height of the V-groove on the mold) × 100%. The PDMS mold is replicated from the nickel master mold. For the molding of precision microstructures, PDMS can completely and directly copy the characteristic dimensions of the microstructure. From Fig. 8, the V-groove thickness of the PDMS mold measured by LSCM is 23.26 μm, and the thickness of the optical glass is 22.46 μm. The replication rate calculated through the formula is 96.6%. The five-point average replication rate of optical glass between 0.5 and 2 kgf/cm² is presented in Table 4. It can be seen from the experimental results that when the embossing pressure is set between 1.5 and 2 kgf/cm², the average replication rate is the highest, reaching more than 94%.

4 Conclusion

Utilizing traditional rigid molds in the rolling process may result in potential cracking due to localized stress on the glass. In response to this challenge, our study introduces a novel approach, utilizing PDMS molds embedded with magnetic particles, including high thermal resistance, elevated hardness, a low thermal expansion coefficient, and outstanding chemical stability. Such characteristics render these magnetic PDMS molds ideal for rolling and embossing optical glass. Employing a single heat source, we simultaneously inductively heat the glass and the mold. This process ensures a minimal temperature difference of only 2.5 °C (± 1.25 °C) between high and low temperatures on the mold surface. Notably, with high thermal resistance, the Ni-PDMS mold exhibits a cooling rate of just 0.27°C/s, markedly superior to conventional metal molds. This capability facilitates precise control over the surface temperature of optical glass, proving highly advantageous for moving roller embossing.

Furthermore, the Ni-PDMS molds preserve PDMS's desirable hydrophobic and low surface energy attributes, which prevents adhesion between the glass and the mold, obviating the need for release agents and ensuring easy detachment from the mold. Our experiment employed a low-power 4.5 kW induction heating approach, elevating the temperature to more than 30 °C higher than the Tg of optical glass. Under an embossing pressure of 1.5 ~ 2 kgf/cm², our experimental results reveal an optimal replication rate surpassing 94%. This innovative approach addresses the challenges associated with traditional metal molds and enhances efficiency and replicability in optical glass roller embossing processes.

Author contributions Ming and Sen-Yeu wrote the main manuscript text, Yao-Yang provided experimental design and comments, Jhao-Hong provided experimental assistance, and all authors reviewed the manuscript.

Data availability No datasets were generated or analysed during the current study.

Declarations

Conflict of interest The authors declare no conflict of interest.

References

Atthi N, Dielen M, Sripumkhai W, Pattamang P, Meananeatra R, Saengdee P, Ter Meulen JM (2021) Fabrication of high aspect ratio micro-structures with superhydrophobic and oleophobic properties by using large-area roll-to-plate nanoimprint lithography. Nanomater 11(2):339

Bona GL, Germann R, Offrein BJ (2003) SiON high-refractive-index waveguide and planar lightwave circuits. IBM J Res Dev 47(23):239–249

Chen P-L, Hong R-H, Yang S-Y (2015) Hot-rolled embossing of microlens arrays with antireflective nanostructures on optical glass. J Micromech Microeng 25(9):095001

Corbari C, Champion A, Gecevičius M, Beresna M, Bellouard Y, Kazansky PG (2013) Femtosecond versus picosecond laser machining of nano-gratings and micro-channels in silica glass. Opt Express 21(4):3946–3958

Darwish MS, Stibor I (2015) Preparation and characterization of magnetite–PDMS composites by magnetic induction heating. Mater Chem Phys 164:163–169

Fang FZ, Zhang XD, Weckenmann A, Zhang GX, Evans C (2013) Manufacturing and measurement of freeform optics. CIRP Ann 62(2):823–846

Haghbin N, Ahmadzadeh F, Papini M (2018) Masked micro-channel machining in aluminum alloy and borosilicate glass using abrasive water jet micro-machining. J Manuf Process 35:307–316

Han R, Lee J, Seong B, Shin R, Kim D, Park C, Kang S (2020) Direct replication of a glass micro Fresnel zone plate array by laser irradiation using an infrared transmissive mold. Opt Express 28(12):17468–17480

Hartmann P, Jedamzik R, Reichel S, Schreder B (2010) Optical glass and glass ceramic historical aspects and recent developments: a Schott view. Appl Opt 49(16):D157–D176

Hsu M-H, Tsai Y-Y, Yang S-Y (2022) Induction heating ferromagnetic particles embedded PDMS mold for microstructure embossing. J Phys Commun 6:025002

Hsu M-H, Tsai Y-Y, He J-W, Yang S-Y (2023b) A double-sided PDMS mold for double-sided embossing by rollers. Microsyst Technol 30:47–54

Hsu M-H, Tsai Y-Y, He J-W, Yang S-Y (2023a) Induction heating of dual magnetic particles embedded PDMS molds for roller embossing applications. Microsyst Technol 29:405–415

Hu M, Xie J, Li W, Niu Y (2020) Theoretical and experimental study on Hot-Embossing of Glass-Microprism array without online cooling process. Micromachines 11(11):984

Kim M, Moon BU, Hidrovo CH (2013) Enhancement of the thermomechanical properties of PDMS molds for the hot embossing of PMMA microfluidic devices. J Micromech Microeng 23(9):095024

Lee H, Binti Kamarudin SNH, Ishak I, Manaf ARA, Jamaludin AS, Shaharudin MAH, Zawawi MZ (2021) Feasibility Study of Wafer Scale Laser Assisted Thermal Imprinting of Glass Nanostructures. In Recent Trends in Manufacturing and Materials Towards Industry 4.0: Selected Articles from iM3F 2020 Malaysia 917–923

Li K, Xu G, Luo H, Liu X, Gong F (2020) Glass flow behaviors in microchannels during hot embossing. Ceram Int 46(13):21517–21526

Li J, Yang K, Lian G, Gong F, Yang G (2023) A novel hot embossing process for producing high-quality glass micro-pillar arrays. J Clean Prod 421:138509

Luo H, Zhang Y, Yu J, Dong X, Zhou T (2023) Additive, subtractive and formative manufacturing of glass-based functional micro/nanostructures: a comprehensive review. Mater Des :112285

Nievas N, Pagès-Bernaus A, Bonada F, Echeverria L, Abio A, Lange D, Pujante J (2022) A reinforcement Learning Control in Hot Stamping for Cycle Time optimization. Mater 15(14):4825

Park Y-K, Joo J-Y, Lee C, Lee S-K (2013) Design and fabrication of a light emitting diode-based diffuser sheet-less light guide plate for lighting applications. Int J Precis Eng Manuf 14:1017–1022

Peng Z, Zhang Y, Choi CLR, Zhang P, Wu T, Chan YK (2023) Continuous Roller Nanoimprint: Next Generation Lithography. Nanoscale 15:11403–11421

Rezem M, Günther A, Rahlves M, Roth B, Reithmeier E (2014) Hot embossing of polymer optical waveguides for sensing applications. Proc Technol 15:514–520

Sah S, Mahayotsanun N, Peshkin M, Cao J, Gao RX (2016) Pressure and draw-in maps for stamping process monitoring. J Manuf Sci Eng 138(9):091005

Sun J et al (2019) Development and application of hot embossing in polymer processing: a review. ES Mater Manuf 6(4):3–17

Tan X, Jiao Q-B, Qi XD, Bayan H (2016) Fabrication of high-efficiency and low-stray-light grating by inductively coupled plasma (ICP) etching-polishing method. Opt Express 24(6):5896–5910

Tsai Y-P, Hung J-C, Yin L-C, Hung C (2012) Ultrasonic vibration-assisted optical glass hot embossing process. Int J Adv Manuf Technol 60:1207–1213

Yan B-H, Wang A-C, Huang C-Y, Huang F-Y (2002) Study of precision micro-holes in borosilicate glass using micro EDM combined with micro ultrasonic vibration machining. Int J Mach Tools Manuf 42(10):1105–1112

Yi A-Y, Chen Y, Klocke F, Pongs G, Demmer A, Grewell D, Benatar A (2006) A high volume precision compression molding process of glass diffractive optics by use of a micromachined fused silica wafer mold and low Tg optical glass. J Micromech Microeng 16(10): 2000

Zhao Z-L, Yu H-P, Wu D-M, Liu Y, Zheng X-T, Zhuang J, Jing P-S (2013) Research on the key technology in ultra-precision machining of optical micro V-groove mold roller. Adv Mater Res 712:1563–1567

Zheng Y, Duan J (2011) Materials and fabrication issues of micro V-groove for optoelectronics packaging. Adv Mater Res 295:1330–1334

Zhou T, Yan J, Masuda J, Oowada T, Kuriyagawa T (2011) Investigation on shape transferability in ultraprecision glass molding press for microgrooves. Precis Eng 35(2):214–220